Int. J. Electrochem. Sci., 17**(2022)** Article Number: 220333, doi: 10.20964/2022.03.45

International Journal of ELECTROCHEMICAL SCIENCE
www.electrochemsci.org

Synthesis and Characterization of Ni(II), Cu(II), Zn(II) and Azo Dye Based on 1,10-*o*-Phenanthroline Binary Complexes: Corrosion Inhibition Properties and Computational Studies

Hamed M. Al-Saidi[1], *Gamal A. Gouda*[2], *Mohamed Abdel-Hakim*[2,*], *Nawaf I. Alsenani*[3], *Anas Alfarsi*[3], *Mahmoud H. Mahross*[2], *O. A. Farghaly*[3], *Shimaa Hosny*[4]

[1]Department of Chemistry, University College in Al–Jamoum, Umm Al–Qura University, 21955, Makkah, KSA.
[2] Department of Chemistry, Faculty of Science, Al–Azhar University, Assiut Branch, 71524, Assiut, Egypt.
[3] Department of Chemistry, Faculty of Science, Al–Baha University, Al–Baha, Saudi Arabia.
[4] Department of Chemistry, Faculty of Science, New Valley University, El–Kharja 72511, Egypt.
[*]E-mail: m.hakim121@azhar.edu.eg

Received: 6 December 2021/ *Accepted:* 9 January 2022 / *Published:* 2 February 2022

Azo dye ligand of *p*[(*p*\-aminosulphonylbenzene)]-azo-5-(1,10)-*o*-phenanthroline L, based on 1,10-o-phenanthroline and *p*-aminosulphonylbenzene with Ni(II), Cu(II) and Zn(II) ion complexes have been prepared and investigated.A potentiometric method was used to determine their stability constants by redox titration in 0.1 M HCl at room temperature. The resulting metal-L species showed the forming molar ratios 1:1 and 1:2. The electrical conductivity values of synthesized metal complexes indicated the semiconducting nature with an activation energy in the range 0.131-0.188 eV. The thermal stability of the [$ZnLCl_2$] is higher than [$CuLCl_2$] and [$NiLCl_2$] complexes. The prepared compounds were tested as mild steel corrosion inhibitors in 1.0 M H_2SO_4 solution using electrochemical analysis (Potentiodynamic polarization technique) and theoretical quantum calculation was studied. The decrease of corrosion current densities and corrosion potential values extracted from Potentiodynamic polarization indicated that all used inhibitors act as a mixed-type inhibitor (decrease each anodic and cathodicTafel slopes). The inhibition efficiency increases for the tested compounds as [$NiLCl_2$] > [$ZnLCl_2$] > [$CuLCl_2$] > L to reach maximum value 92.3 % for [$NiLCl_2$]. The changing in electrochemical descriptors obtained by verifying inhibitors concentration 100, 200 and 400 ppm, improves its adsorption over the surface of mild steel. Inhibition was attributed to the adsorption of the prepared compounds on the surface of the mild steel. The descriptors of adsorption isotherm of the inhibitors were obeyed Langmuir adsorption isotherm. Morphology examination of the surface of mild steel electrodes was tested by scanning electronic microscopy in the presence and without inhibitors. Theoretical investigations were applied to the ligand tested and metal complexes in this study by using Gaussian 09 software program involved optimization by DFT method by DFT/B3LYP/LANL2DZ level. Descriptors calculation such as (E_{HOMO}, E_{LUMO} and energy gap, molecular electrostatic potential shape and counter plots) were obtained by quantum calculation that approve link between excremental and theoretical studied. The complexes were relatively active against pathogenic bacteria such as Gram positive and Gram negative.

Keywords: Azo dye metal complexes; corrosion; DFT calculations; antimicrobial ability.

1. INTRODUCTION

Azo dye of 1,10-*o*-phenanthroline derivatives plays an important role in the development of polypyridyl metal complexes [1, 2]. Complex metal dyes have attracted increasing attention because of their interesting and electronic geometric features related to their applications such as molecular memory storage and printing system [3]. Many publications are devoted to synthesis and characterization of azo dye ligands based on 1,10-*o*-phenanthroline and their metal complexes [4, 5]. Numerous compounds have been studied as corrosion inhibitors and most of the well-known inhibitors are organic compounds containing nitrogen, sulfur, and oxygen atom in their molecular structures. Consequently, nitrogen with heterocyclic compounds is an efficient corrosion inhibitor on steel in acidic environments [6]. Most compounds that have an aromatic ring and heterocyclic atoms are responsible for corrosion inhibition and metal dissolution in the acidic media [7, 8]. Numerous reports have been published in the use of heterocyclic compounds in addition to the presence of polar groups and π-electrons as corrosion inhibitors [9, 10]. The structure of phenanthroline derivatives and the number of possible suggests mechanisms for interaction with metal surface gave them great importance as inhibitors of corrosion [11]. Electrochemical corrosion studies have investigated phenanthroline derivatives using bi-valent metals such as Co(II), Cd(II) and Cu(II) as corrosion inhibitors [12-14].

Quantum chemical calculations have been applied to support experimental findings and detect correlations between molecular chemical structures and the reactivity of molecules that lead to the best corrosion inhibition [15, 16]. Also establish the relation between the inhibitor molecules and iron corroded surface as donor-acceptor system. DFT calculations have carried on complexes of phenanthroline derivatives with hetero ligand and azo-dye ligand [17, 18]. In addition, some research has focused on the use of azo metal complexes as a broad-spectrum antibiotic for Gram-positive and Gram-negative bacteria [19]. The studies were also expanded to include the use of these complexes as an antifungal for various species, not some [18].

In this work, the formation equilibrium were extended to stability constants and the stoichiometry of the complex formation of *p*[(*p*\-aminosulphonylbenzene)]-azo-5-(1,10)-*o*-phenanthroline with metal ions Ni(II), Cu(II) and Zn(II) in aqueous HCl. The physicochemical properties of the synthesized metal-ligand complexes will be investigated by different analytical techniques. The prepared complexes were tested to inhibit corrosion for mild steel in 1.0 M H_2SO_4 solution using electrochemical analysis. Theoretical quantum computation has also been studied. Antibacterial and antifungal activities of prepared metallic compounds are also discussed.

2. EXPERIMENTAL

The chemicals used in this study were analytically grade and used without further purification. Meta chlorides from nickel (II), copper (II) and zinc (II) (Sigma-Aldrich Germany) ions have been

dissolved in deionized water. The concentration of carbon, hydrogen, nitrogen and sulfur in the prepared compounds was determined by a GmbhVario El analyser from ElementarAnalysen system. The mass spectra were performed using the JOEL JMS 600 spectrometer at an ionizing potential of 70 eV using the direct input system. The Fourier transform infrared of all compounds was registered in the 4000-400 cm^{-1} region with a Shimadzu spectrophotometer (Model Nicolet 6700). Spectral measurements of electronic absorption in UV and visible regions were performed in DMF by UV-2102 PC Shimadzu Spectrophotometer with a matched 1 cm quartz cell in the 200-900 nm wavelength range. Magnetic susceptibility measurements were carried out at room temperature by means of a magnetic susceptibility evaluation of the MSB-Auto type. Molar susceptibilities were corrected for the diameter of the constituent atoms by Pascal constants. The calibrate used was $Hg[Co(SCN)_4]$. Thermogravimetric (TG-DTG) by Instrument model: SDTQ600 V20.9 TGA from 40 to 900 ^oC with the heating rate of 20 ^oC min^{-1} under N_2atmosphere. Scanning electron microscope of the complexes were scanned on an instrument of the type Joel JSM 5400 LV.

2.1. Preparation of p[(p\-aminosulphonylbenzene)]-azo-5-(1,10)-o-phenanthroline

The ligand *p*[(*p*\-aminosulphonylbenzene)]-azo-5-(1,10)-*o*-phenanthroline, produced by diazotizing of *p*-aminosulphonylbenzene and then coupling this intermediate to 1,10-*o*-phenanthroline has been synthesized and characterized according to recommended procedures (Figure 1) [5].

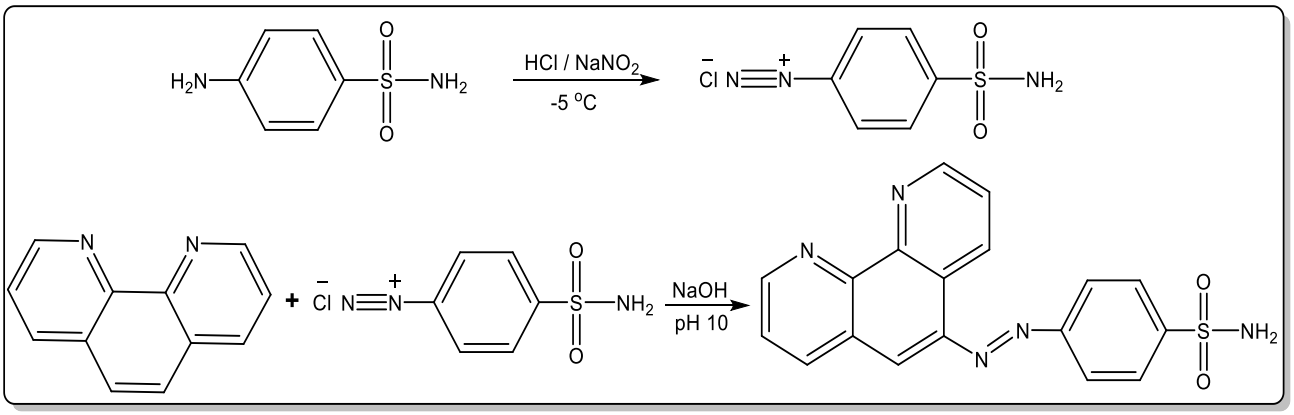

Figure 1. Preparation of *p*[(*p*\-aminosulphonylbenzene)]-azo-5-(1,10)-*o*-phenanthroline.

2.2. Preparation of complexes

The ethanolic solution (20 mL) of *p*[(*p*\-aminosulphonylbenzene)]-azo-5-(1,10)-*o*-phenanthroline (0.1 M, 0.73 g) was mixed with $NiCl_2$, $CuCl_2$ or $ZnCl_2$ salts (0.1 M), then refluxed for about 2 h. The precipitated compounds have been filtered, ethanol washed and air dried. The ligand colour solution was changed from dark yellow to green, dark green and light yellow for the Ni(II), Cu(II) and Zn(II) ion complexes, respectively.

2.3. Mass spectra

The mass spectrometric analysis of compound L reflects the unstability of this compound under electron impact, which suffers extensive skeletal fragmentation to give the listed fragments with high and low relative abundance. In Figures 2 and 3 the fragmentation pathway is characterized by the appearance of azobenzenesulphonyl amine ion $(M\text{-}C_{12}H_8N_2)^+$ with m z^{-1} 184 (5.9 %) and 1,10-*o*-phenanthroline ion $(M\text{-}C_6N_3H_6SO_2)^+$, with m z^{-1} 180 (100 %).

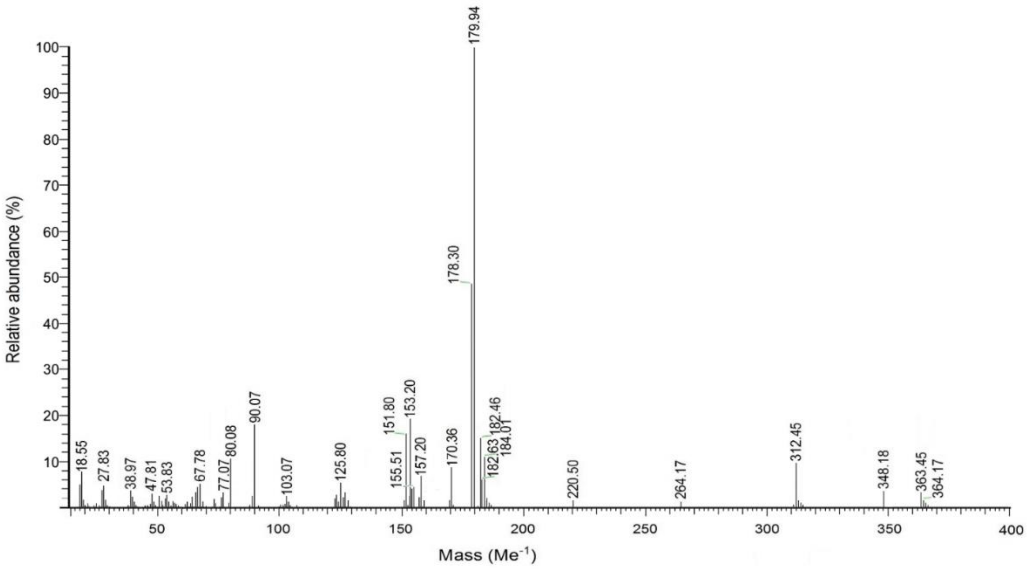

Figure 2. Mass spectrum of azo dye L

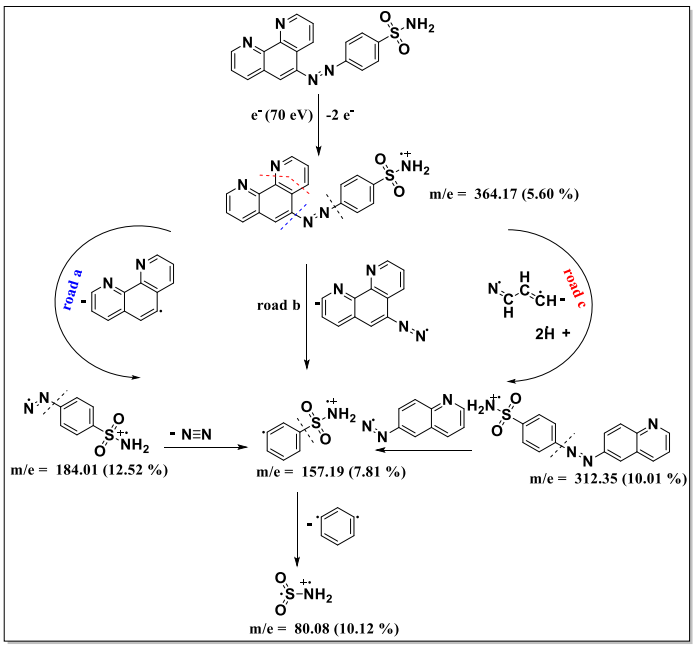

Figure 3. The fragmentation pathway the azo dye ligand, L

2.4. Titration method

The potentiometric titrations were carried out using a 352/252 model, consisting of EG-G Potentiostat-galvanostat (model 273A). A plate of platinum served as the indicating electrode. The redox system composed of L was created by oxidation of a small portion of the initial L into 0.1 M HCl with 0.1 M iodine solution (0.5 mL).

2.5. Electrical measurements

Resistance was measured by a high-strength tester (Keithley, Model 6517B) with a range of 103-1013 Ω. Firstly, a thin layer of L and its complex metallic samples were prepared on a 1.5-3.0 mm thick polished glass disc. Resistance was measured by three samples of each glass. The relative conductivity error was determined to be 4 %. The experimental error in the determination of the activation energy (E_a) for conduction is estimated at less than 0.025 eV. The values for resistivity and conductivity are calculated using (Eq. 1) [20].

$$R = \rho\ (l/A) \quad (1)$$

R; Ohm (Ω); is the resistance, *A; cm*^{2}*;* the cross-sectional zone and *l;* cm; is the thickness of the sample. The resistivity (ρ); Ω cm; of the material is calculated from Eq. 2where σ is the conductivity in Ω^{-1} cm^{-1} and is calculated using (Eq. 2) [19].

$$\sigma = 1/\rho \quad (2)$$

Arrhenius equation plays a major role in conventional chemical kinetics works [19]. It expresses the ratio constant dependency on a wide range of temperatures in terms of only two settings. The E_a is the experimental activation energy in Joules by (Eq. 3):

$$\sigma = A\exp\ (-E_a/\ K_bT) \quad (3)$$

where A is the pre-exponential factor, the Boltzmann's constant is K_b (1.3806×10^{-22} Joule $Kelvin^{-1}$) and T is the temperature in Kelvin.

2.5.1. Preparation of mild steel electrodes

The mild steel electrodes have a square sheet shape with a percentage compositional weight (Mn 40%, C 0.16 %, S 0.10 %, P 0.13 %, S 0.02 % and remaining in the form of iron) has been used in electrochemical polarization studies. The 0.1 cm × 1.0 cm × 0.015 cm of mild steel coupons were washed with soap and water, then surface of mild steel electrodes has been polished successively by different qualities of metallographic emerald papers 1200 and 1400, to obtain on smooth surface prior practice experiments washed with bi-distilled water, using acetone for disinfection and finally dried [21].

2.5.2. Preparation of solution for corrosion investigation

Sigma-Aldrich Laborchemikalien's H_2SO_4 solution (1.0 M, 98 %), used as a corrosive medium in this study. Ligand and its metal complexes were prepared by analytical method to obtain the required concentrations (100, 200 and 400 ppm).

2.5.3. Electroanalysis technique

Electrochemical methods used in this study for description each of open circuit potentials (OCP) at mild steel in the solutions (blank without and with inhibitors solutions) to obtain steady state potential ($E_{s.s}$) which is equal to or nearby corrosion potential ($E_{corr} \approx E_{ocp}$), and potentiodynamic polarization which gives information about descriptors of Potentiodynamic polarization such as corrosion potential (E_{corr}), corrosion rate (CR), corrosion current density (I_{corr}), inhibition efficiency percentage (IE %) and surface coverage (θ). OCP proceed by tow electrodes, reference electrode as (SEC) and working mild steel but in Tafel experiments add counter electrode (Pt wire) with the obvious OCP electrodes. OCP and Potentiodynamic polarization studied by EG-G potentiostat/galvanostat model 273A. Potentiodynamic polarization was measured from ± 250 mV vs. $E_{corr \approx ocp}$ with scan rate 0.3 mV Sec^{-1}. The percentage of IE and CR for the inhibitors studied was calculated from I_{corr} according to the following Eqs. 4 and 5, respectively [21].

$$CR = \frac{0.13 \times I_{corr} \times Eq.Wt}{D \times A} \quad (4)$$

where, the corrosion rate is *CR* (mpy) by millimeters per year, the corrosion current density is I_{corr} (μA cm^{-2}), the equivalent weight of the metal is *Eq. Wt.* (g eq^{-1}), the area is *A* (cm^2), the density is *d* (g cm^{-3}), and the metric and time conversion factor is 0.13.

$$IE\ \% = \frac{CR_1 - CR_2}{CR_1} \times 100 \quad (5)$$

where, CR_1 and CR_2 are the free and inhibited corrosion rates, respectively.

2.6. Quantum calculation studied

Optimization of the studied L ligand molecular structures and their metal complexes [NiLCl2], [CuLCl2] and [ZnLCl2] were performed by Gaussian 09 software by using Universal Molecular Force Field Mechanics (UFF) method [22, 23]. Subsequently, point energy calculations were carried out with the theoretical level DFT/B3LYP/LANL2DZ via optimized structures using UFF. Based on point energy calculations, some parameters of the calculated quantum chemistry of the inhibitors were extracted as the lowest unoccupied molecular orbit energy (E_{LUMO}), the highest molecular orbital

energy occupied (E_{HOMO}), the energy gap (E_g) between E_{HOMO} and E_{LUMO}, global hardness (η), softness (σ), overall electrophilicity (ω) and the fraction of transferred electrons (ΔN).

2.7. Antimicrobial activity of the prepared compounds

Antimicrobial activity of the synthetic compounds was determined through Gram-negative; *P. aeruginosa* and *E. coli*; and Gram-positive bacteria; *B. subtilis* and *S. aureus*. Also, pathogenic fungal strain; *A. niger*, *A. flavus*, *C. albicans* and *f.oxysporum*, was also used to study the antimicrobial activity of metal complexes. 50 µL in various concentrations (75, 100 and 150 µg/mL) of Ni(II), Cu(II) and Zn(II) metal complexes in dimethyl sulfoxide (DMSO) has been used for Gram positive and Gram negative, and pathogenic yeasts. To get a positive check, Cefepime was used as an anti-bacterial standard, whereas fluconazole was used as an antifungal standard in relation to the negative aqueous blank test of the DMSO solvent. All experiments were incubated at 37 degrees Celsius for 24 hours. Bacterial and fungal cultures were obtained from the Mycological Centre of the University of Assiut, Assiut, Egypt.

3. RESULTS AND DISCUSSION

The stepwise metal complexes were investigated with the help of the Bjerrum method [24, 25]. In this respect, the redox system is made up of the ligand (2.59×10^{-2} M) in 0.1 M HCl and its oxidized shape titrated with a solution of metal ions (7.50×10^{-2} M) in 0.1 M HCl. The concentration of the equilibrated ligand ([L]) and the formation function ($\bar{n}$) at each titration point was computed with (Eqs. 6, 7):

$$\log [\boldsymbol{L}] = \frac{E_I - E_i}{1.9837 \times 10^{-4} T} + \log C_L + \frac{1}{2} \log \frac{V_I}{V_T} \quad (6)$$

$$\bar{n} = \frac{C_L - [\boldsymbol{L}]}{C_M} \quad (7)$$

where, E_I and E_i constitute the initial equilibration potentials of the system in the absence of metal ions and at the current titration point, T is the temperature in Kelvin°, C_L is the primary concentration of the ligand, V_I and V_T are the starting and total volumes, respectively, and C_M is the metal ion concentration (7.50×10^{-2} M) for each titration point. These results were analyzed by *Excel & Origin* programs using titration data, and then constant stability values were computed [24, 26, 27]. In this work, the data show that the equilibration potential of the redox system increases in the potentiometric titration process when the volume of metal ions added to a standard solution increase. During titration, no precipitation developed, indicating that there is no trend to hydrolysis [27]. Figures 4 and 5 showed potentiometric titration formation curves of metal ions complexes with L at room temperature in 0.1 M HCl. Potentiometric titration curves (Figure 5) showed that metal-L complexes in 0.1 M HCl produced two 1:1 and 1:2 molecular ratios (metal : L).

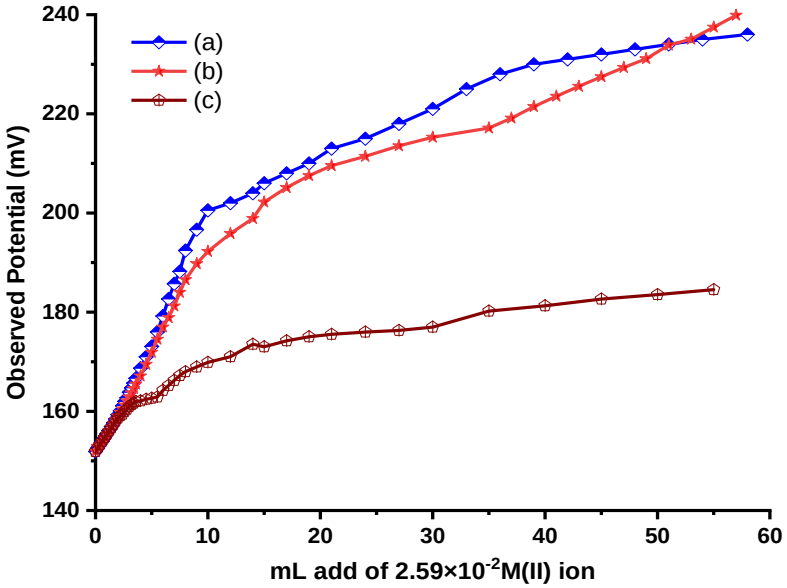

Figure 4. Titration of 50 mL of L (2.59×10^{-2} M) with (a) copper (II), (b) nickel (II) and (c) zinc (II) ions (7.50×10^{-2} M) species in 0.1 M HCl

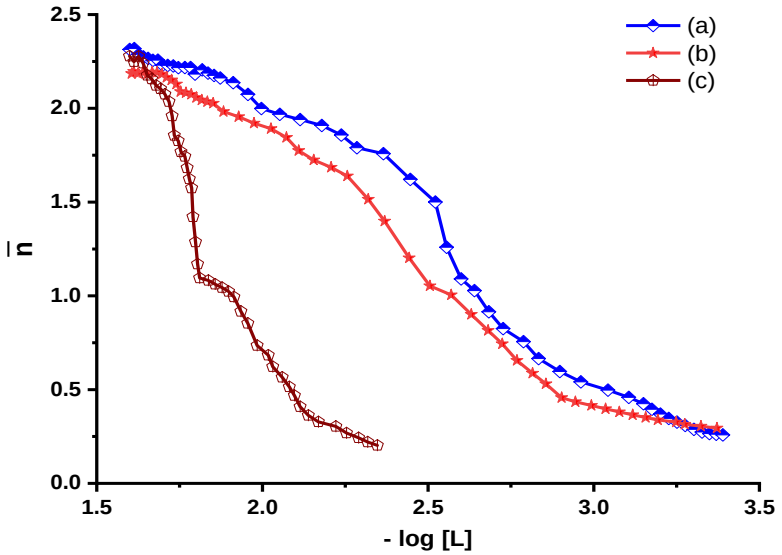

Figure 5. Formation function of species (metal-L): (a) copper (II), (b) nickel (II) and (c) zinc (II) ions in 0.1 M HCl

3.1. The precision of experimentally determined log K_i values

The precision of experimental log K_i values is examined by determining the log K_i values of L from two sets of potentiometric titrations. All the experimental conditions are kept identical for two sets of titrations. The calculation methods of standard deviation (SD) of the values (log K_i) were as reported elsewhere [28]. The values of formation constant obtained from potentiometric titrations of metal-L species are presented in Table 1.

Table 1. The stability constants of metal-L species in 0.1 M HCl

Species	log K_1 (SD)	log K_2 (SD)
Ni(II)-L	2.873 (0.011)	2.300 (0.013)
Cu(II)-L	3.037 (0.012)	2.517 (0.082)
Zn(II)-L	2.090 (0.015)	1.790 (0.012)

Table 1 show that with increasing amount coordinated L molecules, log K_i decreases. Stepwise formation constant (log K_1 + log K_2) values were as follows: 5.554 for Cu(II) system, 5.173 for Ni(II) system and 3.880 for Zn(II) system. The Cu(II) complex has the highest stability than Ni(II) and Zn(II) species. These data indicate that the ratio stepwise formation constants are not so large enough, so it was necessary to clarify the estimated constants either successive approximation method or by the pH-meter program [29].

3.2. Characterization of the isolated solid complexes

Binary complexes of Ni(II), Cu(II) and Zn(II) ions with L ware prepared by the interaction of this ligand with the respective metal salt according to the following (Eq. 8):

$$L + MCl_2 \rightarrow [MLCl_2], \text{ where M = Ni(II), Cu(II) or Zn(II)} \quad (8)$$

All the complexes are partially soluble in methanol, ethanol, acetone and chloroform, but soluble in dimethyl sulphoxide (DMSO), and dimethyl formamide (DMF). Molecular formula, molecular weight, colour elemental analysis and decomposition points (m.p.) of the compounds are tabulated in Table 2.

Table 2. Physical and elemental analysis of the solid L and its metal complexes

Compound M.F. (M.Wt.)	Colour	m. p., °C	Microanalysis found (calculated)			
			% C	% H	% S	% Cl
L $C_{18}H_{13}N_5O_2S$ (363.39)	Pale brown	198	58.81 (59.49)	3.63 (3.61)	8.90 (8.82)	- -
$[NiLCl_2]$ $C_{18}H_{13}N_5O_2SNiCl_2$ (490.95)	Brown	202	43.92 (43.85)	2.67 (2.66)	6.53 (6.50)	14.41 (14.38)
$[CuLCl_2]$ $C_{18}H_{13}N_5O_2SCuCl_2$ (497.85)	Dark brown	204	43.52 (43.43)	2.67 (2.63)	6.72 (6.44)	14.81 (14.24)
$[ZnLCl_2]$ $C_{18}H_{13}N_5O_2SZnCl_2$ (501.70)	Reddish brown	213	43.17 (43.09)	3.07 (3.01)	6.42 (6.39)	14.21 (14.13)

3.2.1. IR spectra

Table 3.IR spectral data of the solid metal complexes (cm^{-1})

Compound	ν(N=N)	ν(NH_2)	ν(*o*-phen)	ν(SO_2)$_{sym}$	ν(SO_2)$_{asym}$	ν(C-H)$_{arom}$	ν(M-N)
L	1441 m	3337 s 3271 s	719 m 869 s 1513 m	1117 s	1362 m	800 s	-
[$NiLCl_2$]	1445 m	3334 s 3271 s	718 s 865 s 1542 s	1172 s	1383 s	779 s	515 m
[$CuLCl_2$]	1452 m	3335 s 3270 s	713 s 873 s 1534 w	1164 s	1379 m	780 s	517 m
[$ZnLCl_2$]	1451 m	3331 s 3270 s	716 s 868 s 1537 s	1177 s	1380 s	775 s	505 m

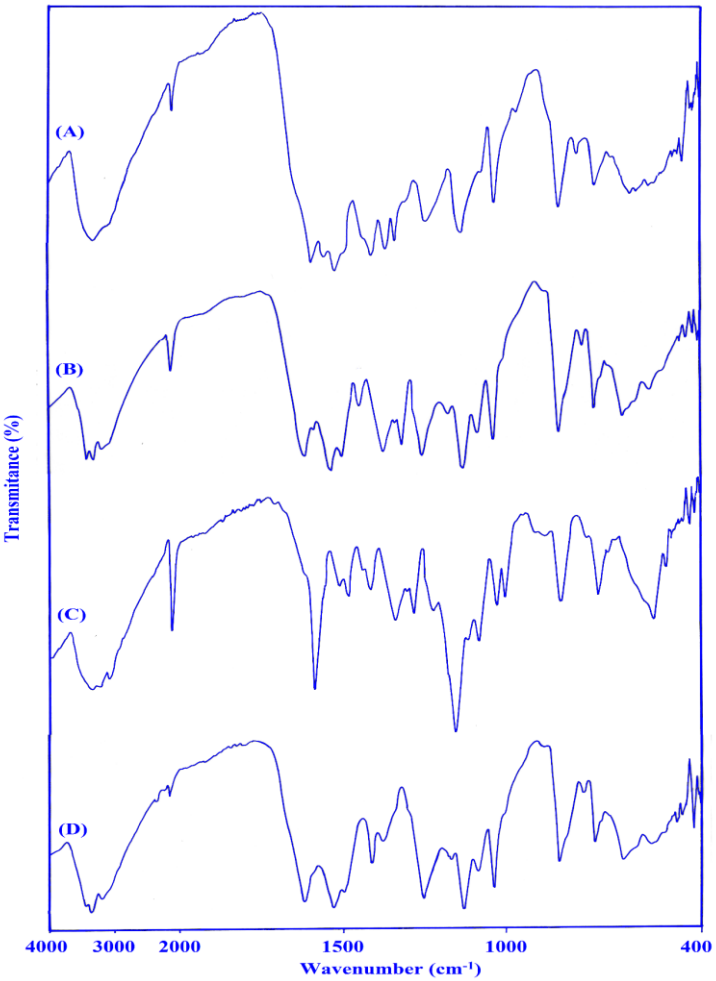

Figure 6. IR spectrum of the solid L ligand (A) and its metal complexes [$NiLCl_2$] (B), [$CuLCl_2$] (C), and [$ZnLCl_2$] (D)

The main infrared spectrum bands of L and its metallic complexes are presented in Table 3 and Figure 6. The L spectra and their metal complexes show a band in the area 1440-1455 cm^{-1} which may be assigned to ν(N=N) a fraction of azobenzene. This absorption frequency range is basically the same for free ligand as in complexes, therefore excluding the coordination of the metallic ion with the azo group. The amino group, ν(NH_2) of the azobenzenesulphonylamine is found in the interval 3265-3340 cm^{-1}. No changes were observed for ν(NH_2) in ligand complexation, other than this coordination with metal ions. Two bands are within range 1115-1175 cm^{-1} and 1360-1385 cm^{-1} that are dedicated to absorption of $\nu(SO_2)_{sym}$ and $\nu(SO_2)_{asym}$, respectively [30]. The absence of an observable shift in the frequency of stretching -SO_2 in the spectra of the compounds with respect to that of the ligand shows that the sulfonyl group is not interacting with the Ni(II), Cu(II) and Zn(II) ions. The L ligand shows multiple bands within the ranges 710-875 cm^{-1} and 1510-1535 cm^{-1} corresponding to the *o*-phenanthroline moiety [30]. The metal-nitrogen connection results in the appearance of a band at 515, 517 and 505 cm^{-1} due to νNi-N, νCu-N and νZn-N, respectively [31]. This is evidence of coordinating the metal ions with ligand through the nitrogen atoms of o-phenanthroline fraction.

3.2.2. Electronic spectra

Electronic spectral data for complexes prepared in the DMF are provided in Table 4. The ligand electron spectrum show the absorption bands to 37,950 and 43,763 cm^{-1} that can be assigned to n-π* and π-π* transition, respectively [32].

Table 4. Spectral, conductivity and electron magnetic moment data of the prepared compounds in DMF

Compound	ν max (cm^{-1})	Band assignment	Molar conductance (S cm^{-1})	μ_{eff} (B.M.)
L	37,950	n-π^*	-	-
	43,763	π-π^*		
[$NiLCl_2$]	38,728	π-π^*	2.74	3.87
	35,231	*n*-π^*		
	24,096	Charge transfer		
	17,668	*d-d*		
[$CuLCl_2$]	36,363	π-π^*	4.58	4.21
	33,738	*n*-π^*		
	24,094	Charge transfer		
	20,619	d-d		
[$ZnLCl_2$]	40,291	Charge transfer	1.87	Dia magnetic
	35,714	π-π^*		
	31,250	n-π^*		

The electronic spectral data of the Ni(II), Cu(II) and Zn(II) ions complexes in DMF display a number of bands in the UV-VIS region. The highest energy band, observed in the range 35,714-38,728

cm^{-1}, is assigned to π-π* transition. The band appearing in spectra of most of the complexes of the interval 24,096-40,291 cm^{-1} is assigned for a charge transfer. The d-d bands in the complexes occur in the interval 17,668-20,619 cm^{-1} indicating that the compounds have a tetrahedral structure surrounding the metal ions [33].

3.2.3. Conductance and magnetic susceptibilities

The $[NiLCl_2]$ complex display effective magnetic moment about 3.87 B.M., (Table 4), which may indicate the tetrahedral structure of the complex [34]. Tetrahedral Ni(II) complex has a triplet T_1 ground state and a large spin-orbit coupling contribution to the moment is expected [35]. The value of the actual magnetic moments to the copper complex is found in 4.21 B.M., and a tetrahedral structure is thus assigned to this complex [36]. The magnetic moment is around 4.21 B.M.; which is closely related to the single spin value for the unpaired electron [37]. Zn(II) complex is found to be diamagnetic as expected for d^{10} configuration. The conductance behavior shows that the complexes are non-electrolytic, and chlorides being coordinated to the metal center directly.

The coordination of M(II) through L ligand N-atoms should produce complexes which should maintain the stability and redox properties of traditional 1,10-o-phenanthroline complexes [38]. The L ligand was coordinated to a M(II) metal center through the 1,10-o-phenanthrolin binding to form a stable complex (Fig. 7).

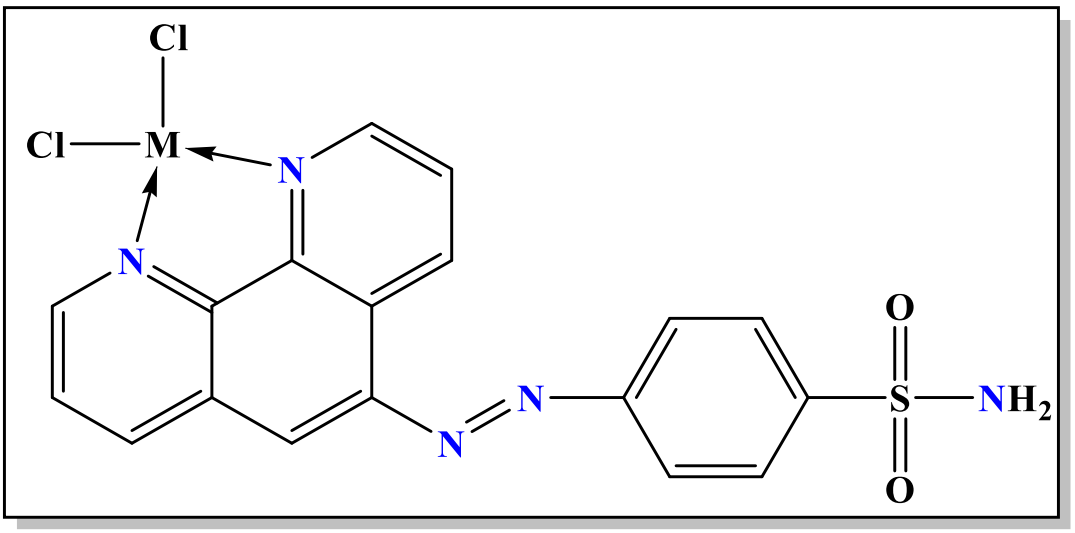

Figure 7. Proposed structure of synthetic metal complexes of the L, where M = Ni(II), Cu(II) and Zn(II) ions

3.2.4. Electrical measurements

The electrical conductivity (σ) of the L and Ni(II), Cu(II) and Zn(II) ions complexes throughout the temperature range 30-90 ºC has been determined; based on the Arrhenius model [39]. Arrhenius diagram of the log (σ) with respect to *1000/T*, where *T* is temperature (K), as illustrated in Figure 8.

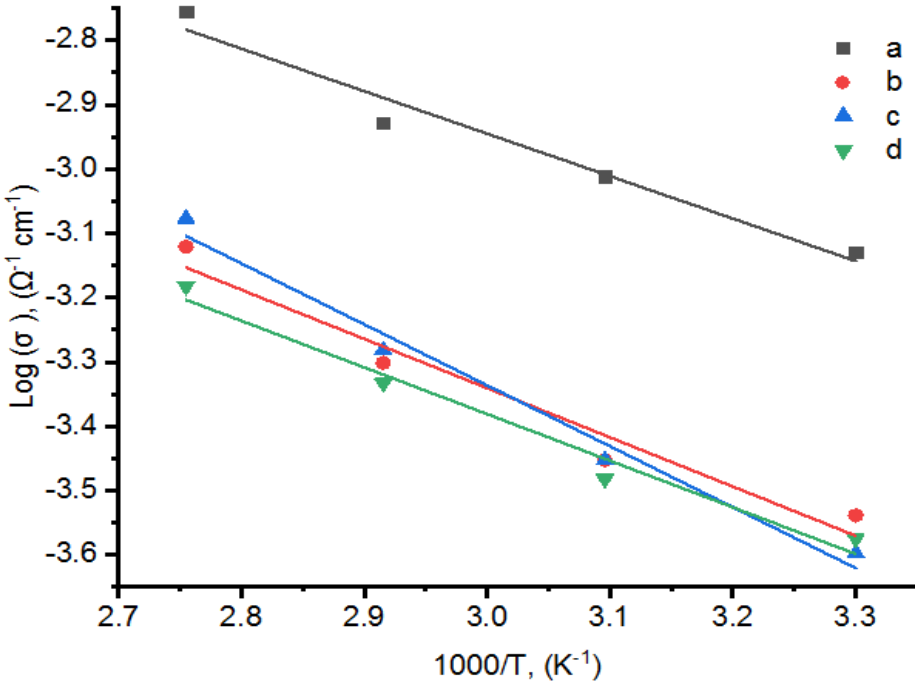

Figure 8. Arrhenius plots of log (σ) vs. 1/T of the L and their metal complexes: a) L, b) [$NiLCl_2$], c) [$CuLCl_2$] and d) [$ZnLCl_2$]

The activation energies (E_a) of the investigated complexes for the conduction process have been determined from the slopes of the Arrhenius parcels and summarized in Table 5. The activation energy values of L, Ni(II), Cu(II) and Zn(II) ions complexes were 0.131, 0.152, 0.188 and 0.144 eV, respectively. This proves that metal compounds are materials with high electrical conduction. These highly conducting metal complexes can have applications in electronics and energy storage applications [40].

Table 5. Electrical data of the L and its metal complexes

Compund	R^2	Slope	E_a(eV)
L	0.966	-0.659	0.131
[$NiLCl_2$]	0.959	-0.764	0.152
[$CuLCl_2$]	0.983	-0.947	0.188
[$ZnLCl_2$]	0.975	-0.724	0.144

It's clear from the observed electrical conductivity and temperature relationship; increasing in a temperature increase in electrical conductivity (Table 5). This behavior assures that the prepared metal complexes are semiconductors [41]. The electrical conductivity values for L and Ni(II), Cu(II) and Zn(II) metal compounds at different temperatures are within the range 9.79×10^{-4} to 1.18×10^{-3} S cm^{-1}. Low electrical conductivity as shown in Table 5 can be attributed to low molecular weight, that makes the degree of conjugation weak or unwanted morphology caused by pressing the sample into hard and

brittle pellets [42]. The activation energy of L and metal complexes proceeded in order Cu(II) > Ni(II) > Zn(II) > L.

3.3. Thermal analysis

The aim of the present thermal analysis study is to obtain information including the effect of temperature on the metal complexes [43-46]. The metal complexes under study were subjected to TG-DTG, and the weight loss was measured from the ambient temperature up to 800 ^{o}C by controlling heating rate 20 ^{o}C per min under nitrogen atmosphere. In general the thermal decomposition of the metal complexes proceeds through many thermal events (two and three). Thermal decomposition of the compounds (Fig. 9) indicates that there is no hydration water associated with the compounds and that the [$ZnLCl_2$] is more thermally stable than [$CuLCl_2$] and [$NiLCl_2$]. The thermal data for metal complexes were given in Table 6.

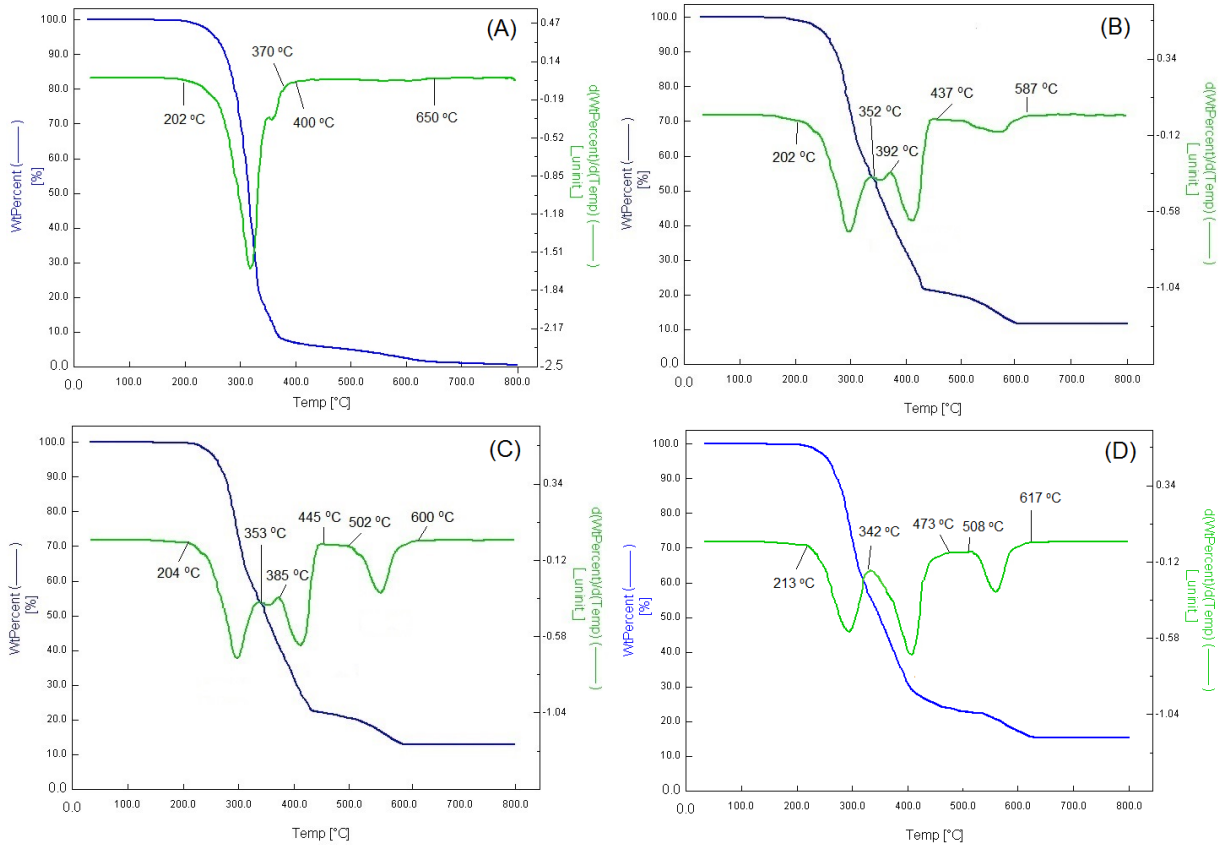

Figure 9. TG–DTG curves of the L ligand (A) and its metal complexes [$NiLCl_2$] (B), [$CuLCl_2$] (C), and [$ZnLCl_2$] (D)

Table 6. Results of thermogravimetric analysis (TGA-DTG) of metal complexes

Compound	Step	Temperature range (°C)	Mass loss in wt. %
L	1st	202-370	91
	2nd	400-650	9
[NiLCl$_2$]	1st	202-350	47
	2nd	390-437	31
	3rd	437-587	9
[CuLCl$_2$]	1st	204-353	46
	2nd	385-445	32
	3rd	502-600	9
[ZnLCl$_2$]	1st	213-342	43
	2nd	342-437	35
	3rd	508-617	8

3.4. Open circuit potential results (OCP)

Figure 10 illustrates the relationship between the voltage E (V vs. (SCE)) of mild steel and the time t (min.) of 1.0 M H_2SO_4 with different concentrations of ligand and the it's metal complexes (100, 200 and 400 ppm). Table 7 presents the data of $E_{s.s}$ for the blank solution without and at different concentrations of the inhibitors investigated. It is evident that the $E_{s.s}$ values for the blank solution have been shifted towards a slightly positive voltage (-0.493 V), indication of the formation of a layer of oxide on the surface of the Mild steel electrode. The addition of various concentrations of ligand complexes and metal to the aggressive medium, $E_{s.s}$ values have been clearly shifted towards positive tension relative to $E_{s.s}$ of the blank (less than - 0.493 V). This change can be attributed to the adsorption of a layer of inhibitory molecules on the mild steel surface, which can directly modify the anodic or cathodic corrosion reaction.

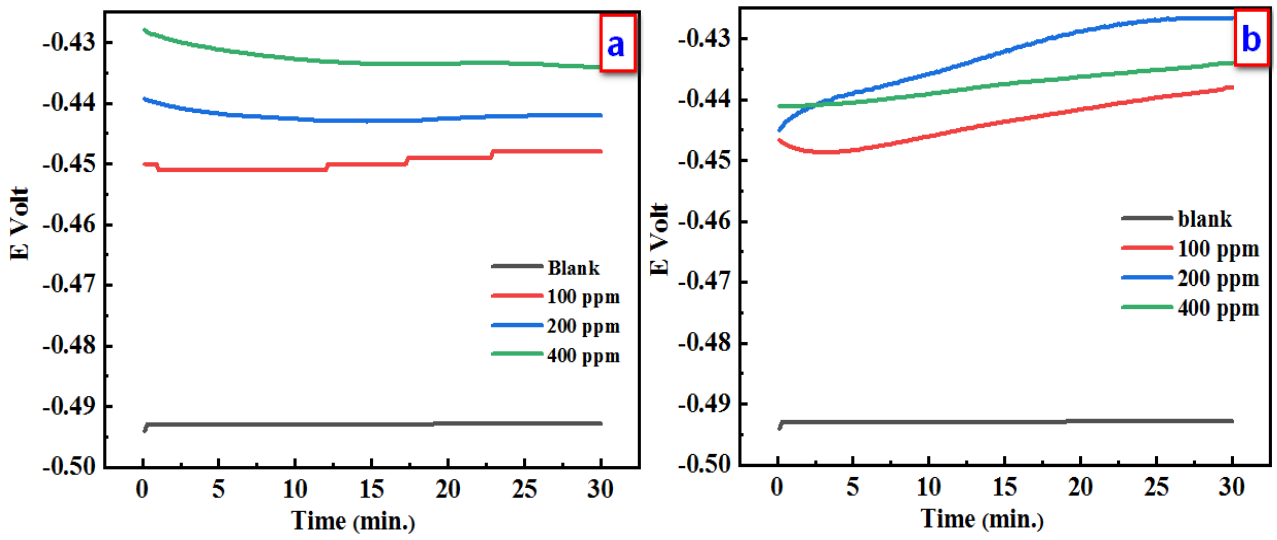

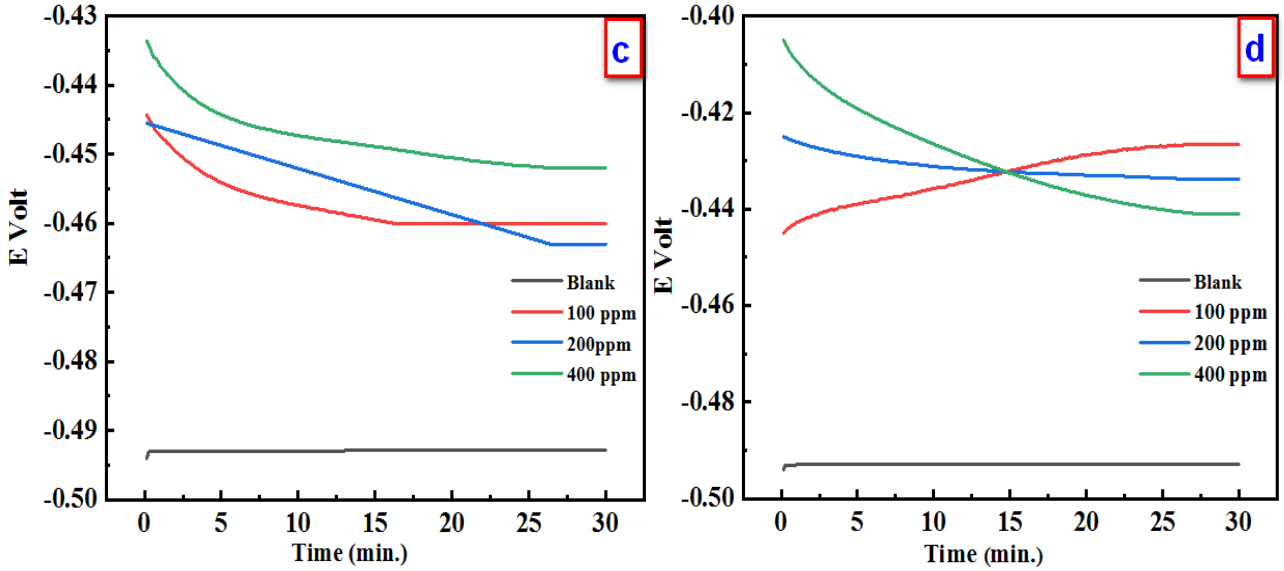

Figure 10. Shows potential E (V) against time (min.) for mild steel with different concentrations (ppm) of inhibitors in sulphuric acid: a) L, b) [$NiLCl_2$], c) [$CuLCl_2$] and d) [$ZnLCl_2$]

Table 7. Steady state potential for mild steel exposed to different concentration of metal complexes with sulphuric acid

Compound	Media (ppm)	$E_{s.s}$(V)
	1.0 M H_2SO_4	-0.493
	100	-0.448
L	200	-0.442
	400	-0.434
	100	-0.438
[$NiLCl_2$]	200	-0.427
	400	-0.434
	100	-0.460
[$CuLCl_2$]	200	-0.463
	400	-0.452
	100	-0.427
[$ZnLCl_2$]	200	-0.434
	400	-0.441

3.4.1. Potentiodynamic polarization

Potentiodynamic polarization descriptors of the mild steel corrosion without and with ligand and its metal complexes at (100, 200 and 400 ppm) in 1.0 M H_2SO_4 solution are illustrated in Figure 11. The values of E_{corr}, I_{corr}, CR, IE %, and θ for various inhibitors are listed in Table 8. The values of I_{corr} of ligand and its metal complexes decreased at comparison with that in the blank solution,

indicating that these test inhibitors act as effective inhibitors, attributed to the adsorption of the test inhibitors at the mild steel surface in relation to the blank test. The lowest value of I_{corr} (270 µA cm^{-2}) was recorded for the inhibitor solution of complex [$NiLCl_2$] at 400 ppm, exhibiting the maximum IE % (92.3 %) and [$NiLCl_2$] recorded the best value of retarding the corrosion of mild steel electrodes immersion in blank solution. For all E_{corr} of the studied complexes has been displaced towards the positive direction of the voltage compared E_{corr} of the blank solution. This observation indicates the adsorption of inhibitory molecules at active sites in the anodic and cathodic position at the surface of the mild steel electrodes. Normally, if transfers of E_{corr}> 85 mV corresponding to E_{corr} of the blank solution, the inhibitor may conform to the cathodic or anodic type. However, if a E_{corr} of inhibitors shift is less than 85 mV comparing by blank solution, the inhibitors obey to a mixed inhibitor [47].

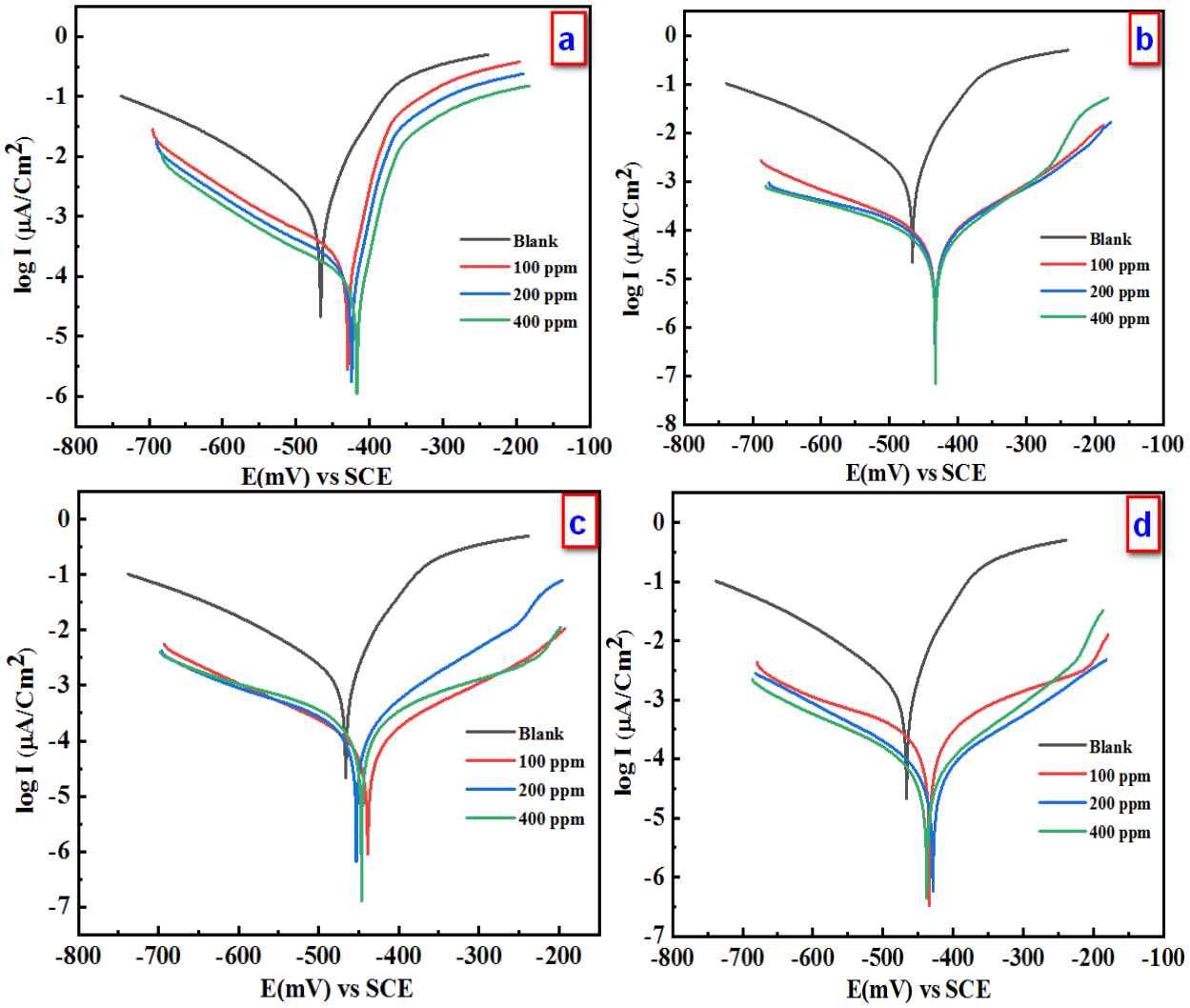

Figure 11. Potentiodynamic polarization of mild steel exposed to various concentrations (ppm) of inhibitors in sulphuric acid: a) L, b) [$NiLCl_2$], c) [$CuLCl_2$] and d) [$ZnLCl_2$]

Table 8. Potentiodynamic polarization descriptors for mild steel exposed to different concentration of tested complexes in sulphuric acid

Compound	Media (ppm)	$E_{corr \approx ocp}$, mV	I_{corr}, µA cm^{-2}	CR, mpy	IE %	Surface coverage (θ)
	1.0 M H_2SO_4	-491	3500	3227	-	-
	100	-448	1050	968	70.0	0.70
L	200	-442	940	867	73.1	0.73
	400	-434	890	821	74.6	0.75
	100	-438	420	387	88.0	0.88
$[NiLCl_2]$	200	-426	385	355	89.0	0.89
	400	-430	270	249	92.3	0.92
	100	-440	605	558	82.7	0.83
$[CuLCl_2]$	200	-443	544	502	84.5	0.84
	400	-444	395	364	88.7	0.89
	100	-428	530	489	84.9	0.85
$[ZnLCl_2]$	200	-430	460	424	86.9	0.87
	400	-434	305	281	91.3	0.91

In this study, the recorded E_{corr} of the inhibitor was shifted to values below 85 mV using E_{corr} of the blank solution, suggesting that all tested metal complexes act as mixed type inhibitors of mild steel in 1.0 M H_2SO_4.

3.4.2. Adsorption isotherm

The current study was utilized the Langmuir isotherm to guess the adsorption behavior of the tested inhibitors, as shown in Eq. 9 [48].

$$\frac{C_{inh}}{\theta} = \frac{1}{K_{ads}} + C_{inh} \qquad (9)$$

where, C_{inh} is different concentrations of tested inhibitors, θ is the surface coverage of mild steel electrodes by molecules of inhibitors and K_{ads} shows the equilibrium constant for inhibition adsorption-desorption processes.

Figure 13 illustrates the Langmuir isotherms thatrepresents C_{inh}/θ with C plots.The K_{ads} was calculated from intercepts these plots and R^2 is correlation coefficient obtained from plots astabulated in Table 9. Data emphasized that the obtainedadsorption was Langmuir isotherms where surface coverage of inhibitors molecules have homogeneity in the distribution of active sites present at the surface of the mild steel. These molecules formed a small layer of thickness at the surface of the mild steel, which attributed to the extract data of values R^2 and slopes nearby unity.Also, retrieved K_{ads} values were used to forecast the standard free energy change (ΔG_{ads}) related to Eq. 10, with followed the valuesin Table 9.

$$\Delta G_{ads} = -2.303RTLog\ K_{ads} \times 55.5 \qquad (10)$$

The verifying in ΔG_{ads} values depends on interaction or attraction between the surface of mild steel and inhibitor molecules.

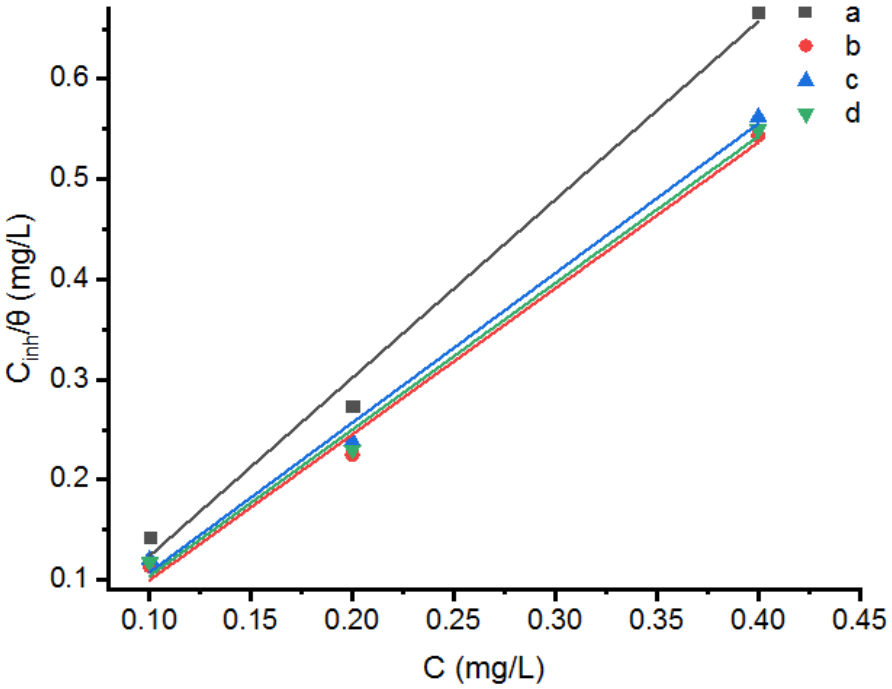

Figure 13. Shows fitting plots for adsorption isotherm of tested L and their metal complexes: a) L, b) $[NiLCl_2]$, c) $[CuLCl_2]$ and d) $[ZnLCl_2]$

Table 9. Show values of adsorption isotherm descriptors for mild steel exposed to different concentration of tested metal complexes in sulphuric acid

Compound	R^2	Slope	log K_{ads}	ΔG, KJ mol^{-1}
L	0.96	0.56	1.08	-16.13
$[NiLCl_2]$	0.96	0.69	1.08	-16.14
$[CuLCl_2]$	0.95	0.68	1.09	-16.15
$[ZnLCl_2]$	0.95	0.66	1.09	-16.16

Table 9 recorded the extracted data of adsorption isotherm; its clear negative sign of ΔG_{ads} indicates the spontaneous adsorption. With revised to adsorption survey, the values of ΔG_{ads} ranged between lower -20 kg mol^{-1} and more than -40 kg mol^{-1}, that describes the type of adsorption isotherm is may be physical or chemical, respectively. As our recorded data, the ΔG_{ads} value ranged between -16.13 kJ mol^{-1} and -16.16 kJ mol^{-1}. This result illustrated and emphasize the adsorption of tested ligand and metal complexes on the surface of mild steel obeyed to physisorption isotherm.

3.5. SEM morphologies

Figure 14(a) shows SEM images of the mild steel surface after elimination or remove the dusty on the mild steel surface.

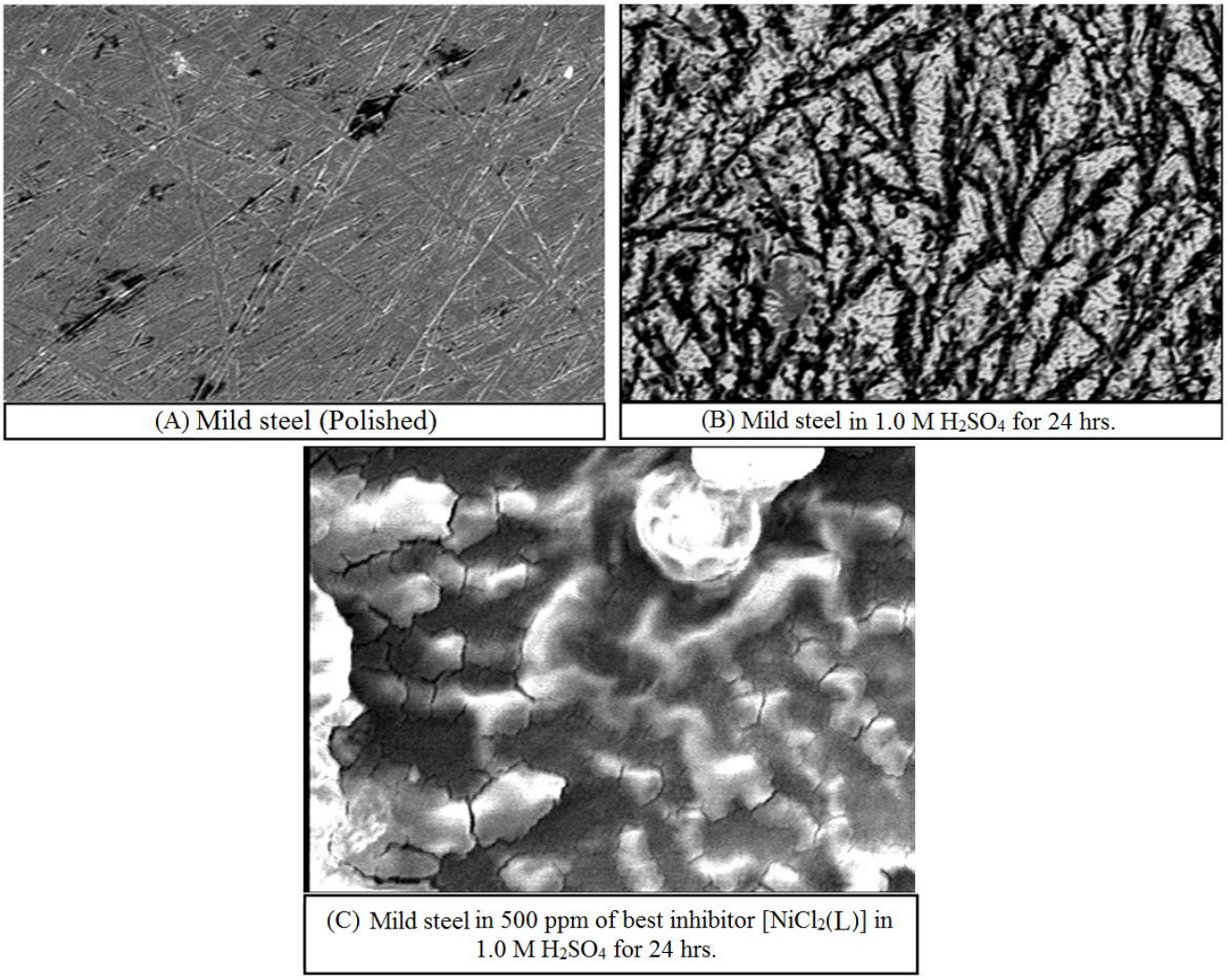

Figure 14. SEM morphology of mild steel electrode (A) immersed in 1.0 M H_2SO_4 (B) and mild steel in [$NiLCl_2$], 500 ppm in sulphuric acid at 50 µm (C)

Figure 14(B) shows the surface of mild steel after immersed at 24 hrs to blank solution of acid, it is observed from that image the surface of mild steel had strongly destroyed and damaged as a result of attack the ions of aggressive media of H^+ and SO_4^{2-} [48]. Figure 14(C) shows image of mild steel surface immersed in blank solution after adding the metal complex that has highest value of IE % for 24 hrs, it's clear, and the attack of acid media to surface of mild steel decreases or delayed to give a protective layer of inhibiting molecules at the surface of the mild steel electrodes.

3.6. Quantum computed

First, the structures of the inhibitors tested have been optimized, and the image of the optimized molecular structure is illustrated in Figure 15. Second step, Frontier molecular orbital was determined and extract some of descriptors that describe the reactivity of the compounds tested, such as the energies of the highest occupied molecular orbit (E_{HOMO}), the lowest unoccupied molecular orbit (E_{LUMO}) and energy gap (EG), as shown in Figure 16. As common from previous researches, if EG has a low value that means the reactivity of this compound, and vice versa as EG is high that means the compound is more stable (less active).

Table 10 recorded the descriptors of quantum calculation for the tested compounds in this study, its clear EG values arranged from lowest to highest values as follow: [$NiLCl_2$], [$ZnLCl_2$], [$CuLCl_2$] and the L. This sequence stated that arranged written from more reactive to less reactive. The reactive complex has highest IE % value than less active complexes, the obtained data theoretically approve the experimental data. Another descriptor which predict the activity of the metal complexes is molecular electrostatic potential (MEP) shown in Figure 17. MEP is also represented as the sites of core love and love of electronic attack. In the obtained MEP, the blue (positive) regions are descriptions of the love electron sites but the red (negative) regions are descriptions for love nucleus attack. All reactivity descriptors equations in this study summarized as reported elsewhere [48, 49].

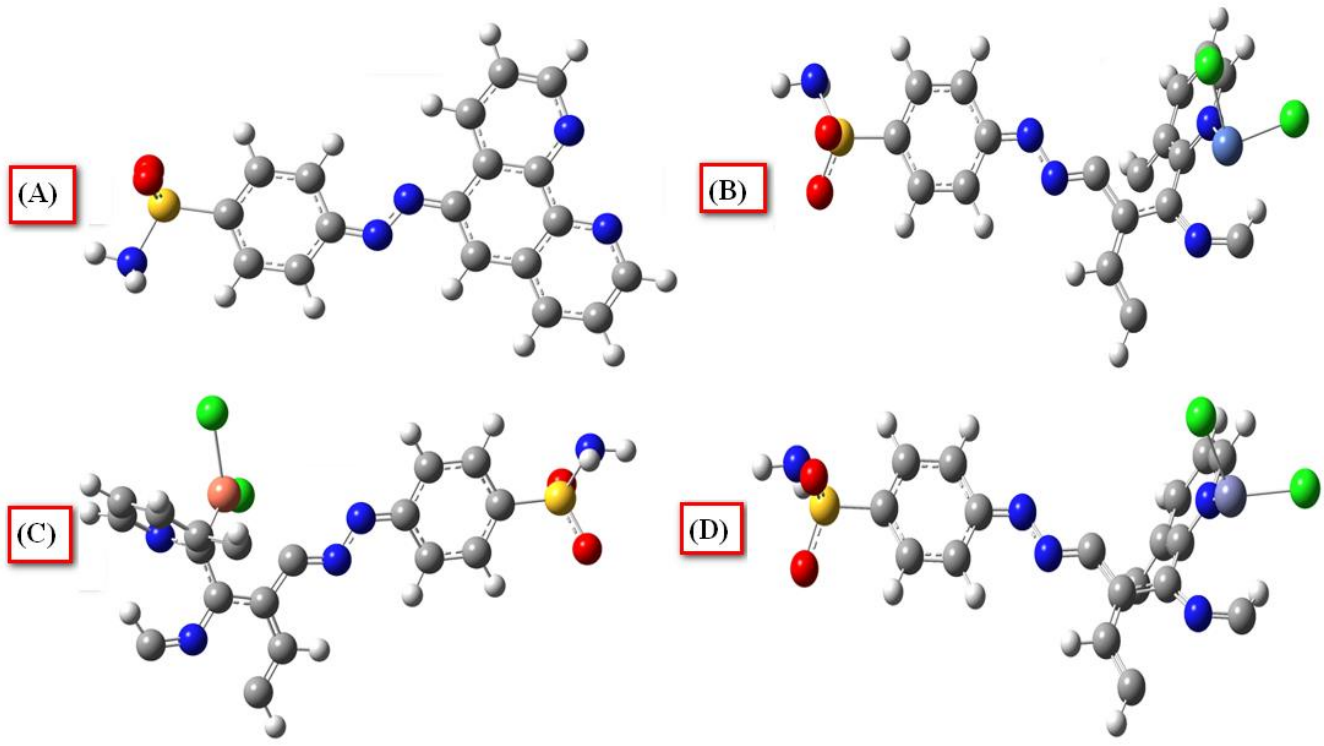

Figure 15. Illustrate optimized structures of tested compounds: (A) L, (B) [$NiLCl_2$], (C) [$CuLCl_2$] and (D) [$ZnLCl_2$]

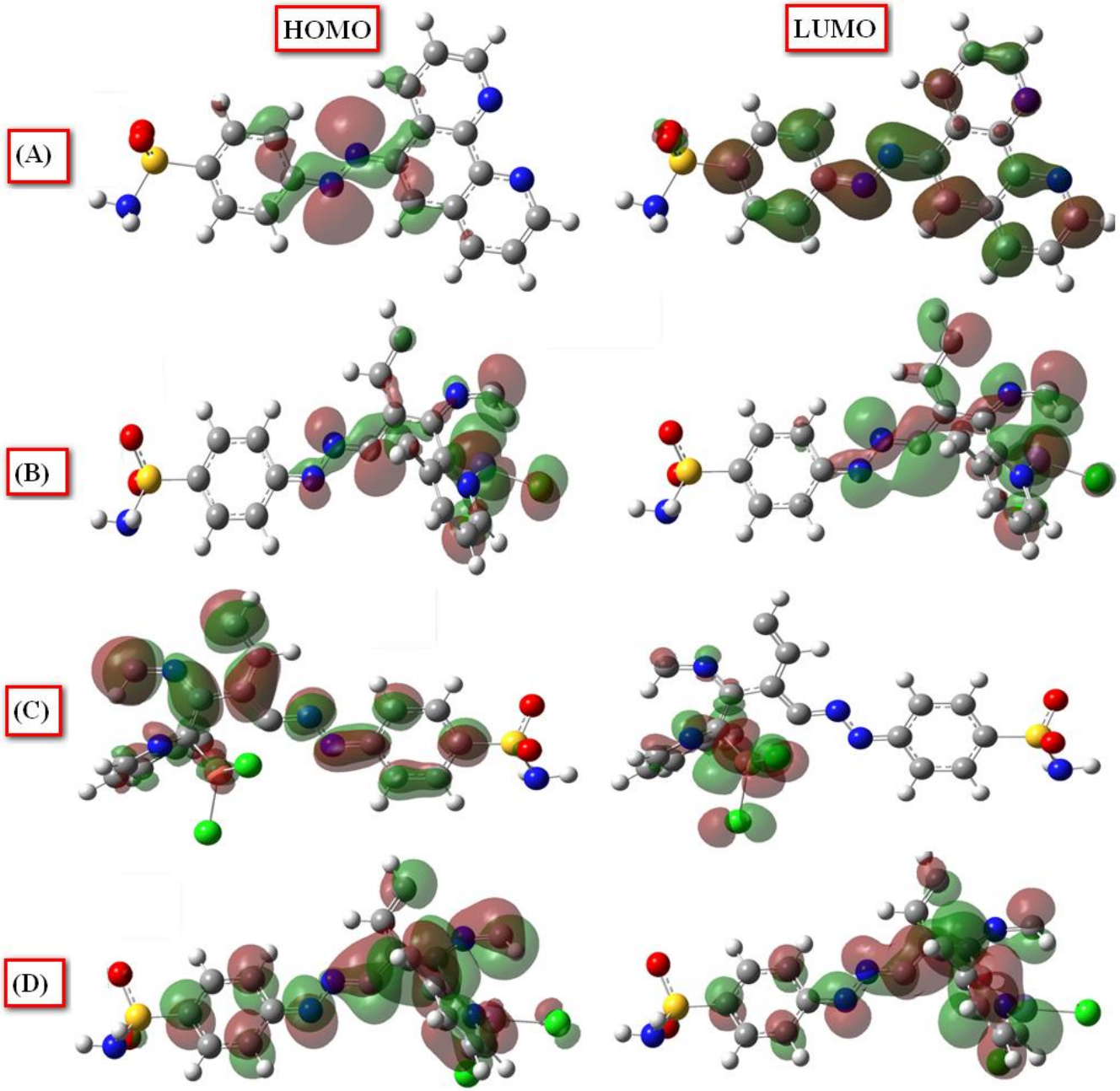

Figure 16. Image of fortier molecular orbitals of tested compounds: (A) L, (B) [$NiLCl_2$], (C) [$CuLCl_2$] and (D) [$ZnLCl_2$]

Table 10. Show descriptors of quantum calculation DFT method by DFT/B3LYP/LANL2DZ level

Compound	E_{HOMO}	E_{LUMO}	EG	η	σ	ω	ΔN	IE %
L	-0.2997	-0.24956	0.0501	0.0250	39.9217	1.5053	-10.9630	73
[$NiLCl_2$]	-0.2504	-0.2467	0.0037	0.0019	537.9	16.6	-133.713	90
[$CuLCl_2$]	-0.2202	-0.20493	0.0153	0.0076	130.8	2.9547	-27.7986	85
[$ZnLCl_2$]	-0.2819	-0.2676	0.0143	0.0072	139.8	5.2768	-38.4103	88

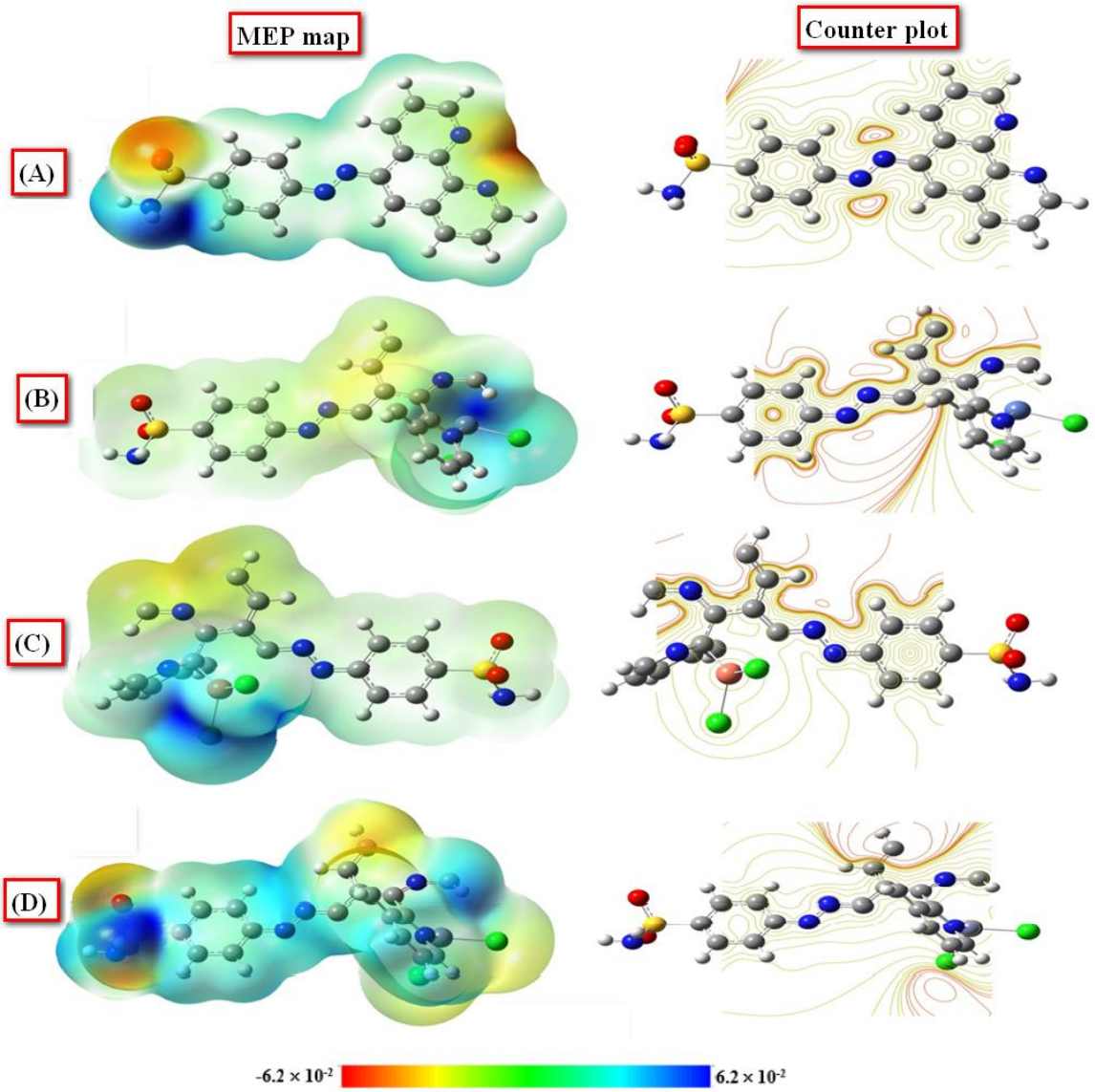

Figure 17. Schematic of MEP map and counter plots of tested compounds: (A) L, (B) [$NiLCl_2$], (C) [$CuLCl_2$] and (D) [$ZnLCl_2$]

In this work, the chemical reactivity indicators were associated with the E_{LUMO} and E_{HOMO} energies. The upper and lower energies of the E_{HOMO} and E_{LUMO} inhibitors studied are due to the better ejection of electrons and gain properties, respectively. As noted earlier, E_{HOMO} and E_{LUMO} were calculated in Table 10. It is notable that the inhibitor studied [$NiLCl_2$] reported an EG less than 0.0037 eV and a hardness (η) less than 0.0019 eV and a softness (σ) greater than 537.9 eV. This lower η value favours the formation of a lower energy barrier for the transfer of electrons between inhibitory molecules and Fe atoms, as well as an internal inhibitory molecule, in which a higher σ value means the opposite. This favors a better interaction behaviour of the inhibitor being studied with the surface of multiple sclerosis. Then it must be pointed out that electrophilicity (ω) was 16.62 eV, suggesting that the inhibitor studied is more love core and less love electron. This finding suggests that this inhibitory molecule is attributed to donor electrons on the surface of mild steel. A further model for linking the inhibition behaviour of the inhibitor observed is that ΔN is -133.7, and it has been reported

that the electron transfer behaviour of this inhibitor is the highest; this action favors efficient adsorption.

3.7. Antimicrobial activity

Metal ligand complexes have a high surface/volume ratio, small dimensions and high dispersive properties, enabling them to interact with microbial surfaces. The wide area of metal complexes improves their interaction with microbes for broad-spectrum antimicrobial activities [50]. To investigate the antimicrobial activity of free ligand and its metal complexes, four types of bacteria and fungi were selected. Bacteria and fungal cells could incubate for 24 hours in the growing medium, containing various concentrations of metal complexes. The inhibit area values are given in Tables 11 and 12. Certain Gram-negative and Gram-positive bacteria exhibit good sensitivity to synthesized metal complexes across the concentration range (75-150 µg mL^{-1}). For a negative control, the absence of a clear zone indicated that standard *Fluconazole* antifungal and some prepared compounds did not have antibacterial or antifungal effects.

Lastly, antimicrobial studies have indicated that the use of complexes can be considered as an alternative strategy for antibiotics to reduce bacterial adhesion [51]. Compared to the medicine *Cefipimus* (150 *µg*), it was obvious to [$CuLCl_2$] (150 µg) is most effective against *B. subtilis*, *S. aureus*, *E. coli* and *P. aeruginosa*. The *Cefipime* inhibiting zones were 18, 12, 7 and 8 mm, respectively. Table 11 and 12summarizes the antimicrobial activities of metal-L complexes against antibacterial standard *Cefipime* and antifungal standard *Fluconazole*. Furthermore, [$CuLCl_2$] at 150 µg had a higher (14 mm) antimicrobial effect than Fluconazole (150 µg mL^{-1}) in inhibiting of growth of *C. albicans*(5 mm). The [$CuLCl_2$] complex showed greater inhibitive activity in bacteria than the fungus. Also, Cu(II) complexes showed improved antibacterial and antifungal activities as compared with their parent azo dye ligand. There are similarities in the results between the present work and other works prepared in different ways [52, 53].

Table 11. Antibacterial activities of the L and its metal complexes measured by the minimum inhibitory concentration in dimethyl sulfoxide (DMSO), (mean ± standard deviation; n = 2)

Microorganisms	L, 75 µg mL^{-1}	Cefipime, 150 µg mL^{-1}	[$CuLCl_2$], 150 µg mL^{-1}	[$NiLCl_2$], 100 µg mL^{-1}	[$ZnLCl_2$], 150 µg mL^{-1}
	Inhibition zone (mm)				
B. subtilis	5 ± 1.25	18 ± 1.44	21 ± 1.23	16 ± 2.01	13 ± 1.77
S. aureus	-	12 ± 1.68	18 ± 1.85	8 ± 2.11	11 ± 1.92
E. coli	-	7 ± 2.02	11 ± 1.74	-	9 ± 1.85
P. aeruginosa	6 ± 1.54	8 ± 1.50	15 ± 1.70	11 ± 1.90	13 ± 1.80

Table 12. Antifungal activities of the L and its metal complexes as determined by minimum inhibitory concentration value in dimethyl sulfoxide (DMSO), (mean ± standard deviation; n = 2)

Microorganisms	L, 75 µg mL^{-1}	Fluconazole, 100 µg mL^{-1}	$[CuLCl_2]$, 150 µg mL^{-1}	$[NiLCl_2]$, 100 µg mL^{-1}	$[ZnLCl_2]$, 150 µg mL^{-1}
	Inhibition zone (mm)				
A. niger	-	-	19 ± 1.25	12 ± 1.77	14 ± 1.05
A. flavus	-	-	16 ± 1.87	16 ± 1.55	5 ± 1.90
f.oxysporum	4 ± 1.82	-	-	-	-
C.albicans	2 ± 1.21	5.03 ± 1.52	14 ± 1.75	7 ± 1.29	10 2.25

4. CONCLUSION

Stability constant of Ni(II), Cu(II) and Zn(II) ion complexes with *p*[(*p*\-aminosulphonylbenzene)]-azo-5-(1,10)-*o*-phenanthrolineazo dye ligand has been investigated using the redox system consisting of the ligand and its oxidized form titrated with a solution of metal ion in 0.1 M HCl. Potentiometric titration curves showed that metal-L complexes in 0.1 M HCl produced two 1:1 and 1:2 molecular ratios (metal:L). The Cu(II)-L has the highest stability than Ni(II)-L and Zn(II)-L species. The prepared complexes of L ligand show distorted tetrahedral geometries. Electronic spectra, magnetic moment and conductance studies prove the assigned geometries. The electrical conductivity show that, the E_a values of the L**,** Ni(II), Cu(II) and Zn(II) metal complexes were 0.131, 0.152, 0.188 and 0.144 eV, respectively. This proves that metal complexes are high-conductive materials and can be used in electronic or energy storage applications. The thermal stability of the $[ZnLCl_2]$ is higher than $[CuLCl_2]$ and $[NiLCl_2]$ complexes. The azo dye ligand L and its metal(II) chelates retard or reduce corrosion of the mild steel in a 1.0 M H_2SO_4 solution. The values of inhibition efficiency were observed to increase as the concentration of inhibitors increasing where the best inhibition efficiency increase for $[NiLCl_2]$ to reach 92.3 %. The inhibitory action was attributed to the adsorption of inhibitory molecules on the test surface. The adsorption isotherm obeys Lanngmuir isotherm. Descriptors obtained from quantum calculations using DFT/B3LYP/LANL2DZ level of theory were correlated to the inhibitive effect of metal complexes. Each experimental and theoretical calculation is in approving. Antimicrobial studies have shown that the use of metal complexes may be continued as an alternative strategy for antibiotics aimed at reducing bacterial adhesion. The Cu(II) complex showed improved antibacterial and antifungal activities as compared with its parent azo dye ligand or Ni(II) and Zn(II) ion complexes.

References

1. A.A.M. Aly, I. Awad, M. Abd El-Mottaleb and K. Abd El-Aal, *Chem. Pap.*, 60(2) (2006) 143-148.
2. T.J. Greenfield, M.M. Turnbull, J. Zubieta and R.P. Doyle, *Inorg. Chim. Acta*, 498 (2019) 119084.
3. M. Adachi, T. Bredow and K. Jug, *Dyes Pigm.*, 63(3) (2004) 225-230.

4. J. Kan, C. Chen, K. Wang, Y. Chen and J. Jiang, *Dyes Pigm.*, 105 (2014) 63-65.
5. M.S. Masoud, A.A. Soayed, A.E. Ali and O.K. Sharsherh, *J. Coord. Chem.*, 56(8) (2003) 725-742.
6. F. Bentiss, M. Traisnel, L. Gengembre and M. Lagrenée, *Appl. Surf. Sci.*, 161(1-2) (2000) 194-202.
7. E.E. Oguzie, *Chem. Eng. Commun.*, 196(5) (2008) 591-601.
8. A.K. Singh and M. Quraishi, *J. Appl. Electrochem.*, 2010, 40(7), 1293-1306.
9. M. Bouklah, A. Bouyanzer and M. Benkaddoor, *Bull. Electrochem.*, 19(11) (2003) 483-488.
10. A. Chetouani, A. Aouniti, B. Hammouti, N. Benchat, T. Benhadda and S. Kertit, *Corros. Sci.*, 45(8) (2003) 1675-1684.
11. V. Agarwala, *Corrosion*, 46(5) (1990) 376-379.
12. T.L. Yusuf, T.W. Quadri, G.F. Tolufashe, L.O. Olasunkanmi, E.E. Ebenso and W.E. van Zyl, *RSC Adv.*, 10(69) (2020) 41967-41982.
13. K. Serbest, T. Dural, M. Emirik, A. Zengin and Ö. Faiz, *J. Mol. Struct.*, 1229 (2021) 129579.
14. I. Papazoglou, P.J. Cox, A.G. Papadopoulos, M.P. Sigalas and P. Aslanidis, *Dalton Trans.*, 42(8) (2013) 2755-2764.
15. J. Fu, H. Zang, Y. Wang, S. Li, T. Chen and X. Liu, *Ind. Eng. Chem. Res.*, 51(18) (2012) 6377-6386.
16. M.Z. Alam, M.S. Alhebsi, S. Ghnimi and A. Kamal-Eldin, *NFS J.*, 22 (2021) 32-40.
17. B.B. Mahapatra, R.R. Mishra and A.K. Sarangi, *J. Saudi Chem. Soc.*, 20(6) (2016) 635-643.
18. A. Stolz, *Appl. Microbiol. Biotechnol.*, 56(1) (2001) 69-80.
19. R. Hassanien, D.Z. Husein and M.F. Al-Hakkani, *Heliyon*, 4(12) (2018) e01077.
20. K.I. Aly, O. Younis, M.H. Mahross, O. Tsutsumi, M.G. Mohamed and M.M. Sayed, *Polym. J.*, 51(1) (2019) 77-90.
21. A.S. El Din and N. Paul, *Desalination*, 69(3) (1988) 251-260.
22. L. Hu and U. Ryde, *J. Chem. Theory Comput.*, 7(8) (2011) 2452-2463.
23. F. Fracchia, G. Del Frate, G. Mancini, W. Rocchia and V. Barone, *J. Chem. Theory Comput.*, 14(1) (2018) 255-273.
24. H.M. Al-Saidi, G.A. Gouda and O. Farghaly, *Int. J. Electrochem. Sci.*, 15 (2020) 10785-10801.
25. A. Amindzhanov, K. Manonov, N. Kabirov and G.A.H. Abdelrahman, *Russ. J. Inorg. Chem.*, 61(1) (2016) 81-85.
26. B.S. Al-Farhan, G.A. Gouda and O. Farghaly, A. El Khalafawy, *Int. J. Electrochem. Sci.*, 14 (2019) 3350-3362.
27. G.A.H. Gouda and G.A.M. Ali, *Malaysian J. Anal. Sci.*, 21 (2017) 1266-1275.
28. M. Dolaz, M. Tümer and M. Diğrak, *Transition Met. Chem.*, 29(5) (2004) 528-536.
29. G.A. Gouda, M. Shatat, T. Seaf Elnasr and M. Abdallah, *Al-Azhar Bull. Sci.*, 24(2-A) (2013) 141-148.
30. R. Palmer and T. Piper, *Inorg. Chem.*, 5(5) (1966) 864-878.
31. O.E. Piro, G.A. Echeverría, A. Navaza and J.A. Güida, *Inorg. Chim. Acta*, 511 (2020) 119831.
32. C.L. Forber, E.C. Kelusky, N.J. Bunce and M.C. Zerner, *J. Am. Chem. Soc.*, 107(21) (1985) 5884-5890.
33. T.A. Khan, S. Naseem, Y. Azim, S. Parveen and M. Shakir, *Transition Met. Chem.*, 32(6) (2007) 706-710.
34. D.A. Shultz, C.P. Mussari, K.K. Ramanathan and J.W. Kampf, *Inorg. Chem.*, 45(15) (2006) 5752-5759.
35. T.M. Barclay, R.G. Hicks, M.T. Lemaire and L.K. Thompson, *Inorg. Chem.*, 42(7) (2003) 2261-2267.
36. M.M. Bekheit, A.R. El-Shobaky and M.T.G. Allah, *Arabian J. Chem.*, 10 (2017) S3064-S3072.
37. T. Rakha, *Synth. React. Inorg. Met.-Org. Chem.*, 30(2) (2000) 205-224.
38. S. Tosonian, C.J. Ruiz, A. Rios, E. Frias and J.F. Eichler, *Open J. Inorg. Chem.*, 3(1) (2013) 7-13.

39. E. Ibrahim, L.H. Abdel-Rahman, A.M. Abu-Dief, A. Elshafaie, S.K. Hamdan and A. Ahmed, *Phys. Scr.*, 93(5) (2018) 055801.
40. H. Zhou, X. Li, Y. Li, M. Zheng and H. Pang, *Nano-Micro Lett.*, 11(1) (2019) 1-33.
41. A. Pardhi, A. Bansod, A. Yaul and A. Aswar, *Russ. J. Coord. Chem.*, 36(4) (2010) 298-304.
42. M. Patel and S. Patil, *Synth. React. Inorg. Met.-Org. Chem.*, 12(3) (1982) 203-214.
43. A.A. Aly, A.H. Osman, M.A. El-Mottaleb and G.A.H. Gouda, *J. Chil. Chem. Soc.*, 54(4) (2009) 349-353.
44. A.A.M Aly, A.H. Osman, M.A. El-Mottaleb and G.A.H. Gouda, *Bull. Pharm. Sci., Assiut Univ.*, 2008, 31(1), 93-108.
45. A.A.M. Aly, A.H. Osman, M.A. El-Mottaleb and G.A.H Gouda, *Bull. Pharm. Sci., Assiut Univ.*, 29(1) (2006) 134-149.
46. A.H. Osman, A.A.M. Aly, M.A. El-Mottaleb and G.A.H. Gouda, *Bull. Korean Chem. Soc.*, 25(1) (2004) 45-50.
47. E. Ferreira, C. Giacomelli, F. Giacomelli and A. Spinelli, *Mater. Chem. Phys.*, 83(1) (2004) 129-134.
48. M. Ouakki, M. Galai, M. Rbaa, A. Abousalem, B. Lakhrissi, E. Rifi and M. Cherkaoui, *Heliyon*, 5(11) (2019) e02759.
49. Z. Rouifi, M. Rbaa, A.S. Abousalem, F. Benhiba, T. Laabaissi, H. Oudda, B. Lakhrissi, A. Guenbour, I. Warad and A. Zarrouk, *Surf. Interfaces*, 18 (2020) 100442.
50. D. Trombetta, F. Castelli, M.G. Sarpietro, V. Venuti, M. Cristani, C. Daniele, A. Saija, G. Mazzanti and G. Bisignano, *Antimicrob. Agents Chemother.*, 49(6) (2005) 2474-2478.
51. M.F. Al-Hakkani, G.A. Gouda, S.H. Hassan, O.A. Farghaly and M.M. Mohamed, *Acta Pharm. Sci.*, 59(1) (2020) 631-645.
52. M.F. Al-Hakkani, G.A. Gouda and S.H. Hassan, *Heliyon*, 7(1) (2021) e05806.
53. M.F. Al-Hakkani, G.A. Gouda, S.H. Hassan and A.M. Nagiub, *Surf. Interfaces*, 24 (2021) 101113.